ICAS-88-2.7.2

AERODYNAMIC AND STRUCTURAL DESIGN OF THE STANDARD CLASS SAILPLANE ASW-24

L.M.M. Boermans
Delft University of Technology
Faculty of Aerospace Engineering
The Netherlands

G. Waibel
Alexander Schleicher
Segelflugzeugbau
Federal Republic of Germany

Abstract

This paper describes the aerodynamic and structural design of the new high performance Standard Class Sailplane ASW-24.
The aerodynamic chapter deals with the design of respectively: the low drag wing airfoil with artificial tripping device to eliminate drag producing laminar separation bubbles, the wing planform and washout optimized for minimum drag and adequate stall control, the aspect ratio based on cross country performance in various weather conditions, the fuselage shape with optimum contraction and fitted to the streamlines of the wing, the tailplane airfoils with artificial tripping devices, and the wing root fairing and T-tail junction aimed to improve local flow conditions.
The structural chapter deals with the properties of glass, aramide and carbon fibers and fiber epoxy laminates, the selection of materials and hybrid structure of the wing, fuselage and tailplane components, and the structural design of the cockpit sidewalls to increase crashworthiness. Finally, preliminary flight experience since the first flight in December 1987 is described.

1. Introduction

The ASW-24, Figure 1, is a new high performance glider for the FAI Standard Class, built by Alexander Schleicher Segelflugzeugbau, Germany. It is the successor of the ASW-19B which was built by Schleicher for more than 10 years. With the exception of some fittings the ASW-24 is a completely new design of all components. This applies to the aerodynamic shape as well as to the materials used. The aerodynamic design was performed in close cooperation between Alexander Schleicher Segelflugzeugbau and the Delft University of Technology (DUT), Low Speed Laboratory (LSL).

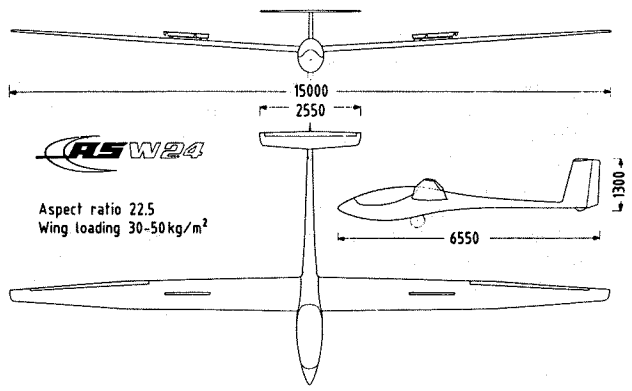

Fig. 1 Three-view drawing of the Standard Class Sailplane ASW-24

Though a large priority was given to the flight performance, a high value was also set to good flight characteristics, active as well as passive safety measures and easy maintenance. It is undisputed that such balance produces the utmost efficiency of the team pilot plus glider.
Adequate horizontal and vertical tail area, elevator and rudder area, and aileron area are provided for good stability and control.
Examples of active safety devices are the automatic connections of all controls at their assembly points, the rubber suspended retractable landing gear with big 5.00-5 wheel and hydraulic disk brake, and the double-panelled airbrakes. Passive safety is provided by progressive strength of the cockpit, where a new design of the cockpit sidewalls combines the visibility of a big canopy with a small cutout of the fuselage structure. The instrument box folds upward for easy getting in and out of the pilot.

The next chapters respectively describe the aerodynamic design of the wing, fuselage and tailplanes taking interference effects into account, as well as the structural design of these components emphasizing the selection of materials and crashworthiness of the fuselage.

2. Aerodynamic Design

Wing

Airfoil

In a previous research program some airfoils were designed such that just by adding material to the surface, the wing of an ASW-19B could be modified and tested in flight [1]. The design of these airfoils was based on experience gained in several investigations: windtunnel experiments on a ASW-19B inner and outer wing segment, analyses of the characteristics of airfoils commonly used in Standard Class sailplanes, comparison of insect impact patterns gathered in flight with seven different sailplanes, windtunnel experiments with real insect remains and with an artificial bug pattern on the leading edge, and windtunnel tests with pneumatic turbulators - blowing air through small orifices periodically spaced in spanwise direction - to eliminate drag producing laminar separation bubbles.
Sailplane performance measurements before and after the wing modification showed the success of the new airfoils with pneumatic turbulators: an improvement in glide ratio over the entire practical flight speed range, varying from 3% to 9%, and no change in minimum flight speed in case of a wet wing were established.
Since this research program several airfoils have been windtunnel tested at LSL, some of them in close cooperation with DFVLR Braunschweig, and attention has been paid to efficient means to pro-

voke transition and eliminate the detrimental effects of laminar separation bubbles [2]. The search for an easy to apply and cheap tripping device resulted in the so-called "zig-zag tape" [3].

The airfoil designed for the ASW-24 is a further development of the airfoil designed for the modification of the ASW-19B inner wing. While the thickness of the latter airfoil was limited to 17.6%c as it had to fit around the existing wing, the new airfoil, named DU84-158, has a thickness of 15.8%c.

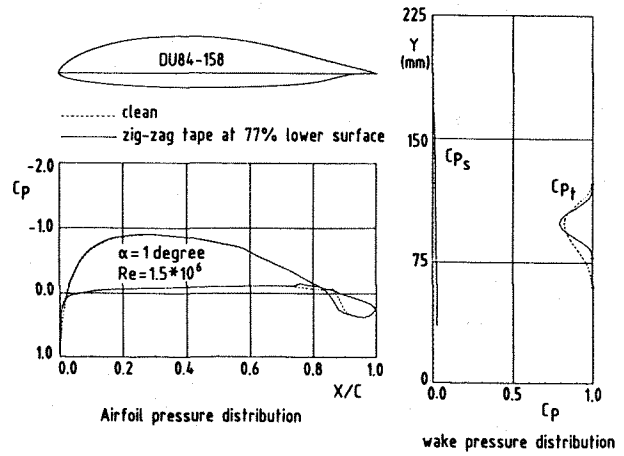

Fig. 2 Measured airfoil and wake pressure distributions

As shown in the measured pressure distributions of Fig. 2, the destabalizing region concept was applied on the upper surface to avoid laminar separation bubbles. Also, the upper surface was designed for a long laminar flow region in case of a clean airfoil, while keeping the performance loss in case of a contaminated leading edge (insects, rain) within reasonable limits. The lower surface was designed to have laminar flow up to 80%c; the succeeding detrimental laminar separation bubbles are eliminated by zig-zag tape. This example of measured surface and wake rake pressures indicates a laminar separation bubble on the lower surface between 80%c and 90%c, as well as its elimination due to zig-zag tape (positioned between 75%c and 77%c) and the corresponding wake drag reduction of 27%.

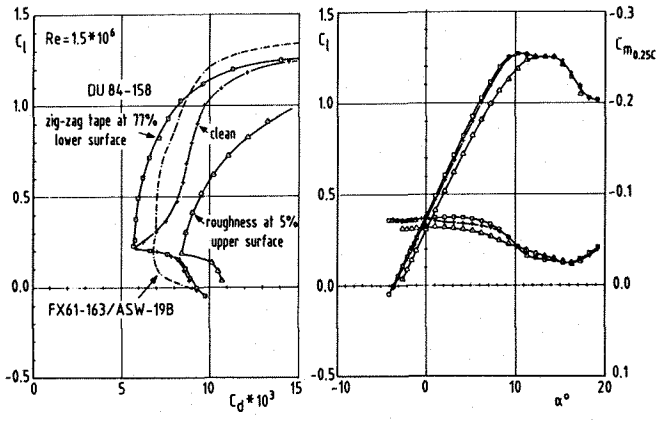

Fig. 3 Measured aerodynamic characteristics

Fig. 3 shows the need and effectiveness of the zig-zag tape. The maximum lift coefficient is practically unaffected by roughness and the stalling behaviour is gradual. The moment coefficient is about 25% less than earlier airfoils used in Standard Class sailplanes [4].
In comparison to the airfoil applied in the ASW-19B inner wing, Fig. 3, the new airfoil has considerably lower drag at lift coefficients below $c_l \approx 1$, i.e at interthermal penetration speeds. Considering optimal penetration speeds in relation to practical climb speeds in thermals and the possibility to use waterballast (up to 170 liter), the lower end of the low drag bucket was designed at $c_l = 0.31$ for Re = 3 * 10E6 (c_d = .0047).

The windtunnel model was provided with a 15% chord flap to simulate the aileron. Experiments showed that the drag produced by the slots was eliminated by flexible sealings fitted flush with the wing and sliding on the aileron upper and lower surface: the measured drag was equal to the drag of a smooth airfoil shape.
Fig. 4 shows some results of tests with different position and thickness of the zig-zag tape, indicating that the tripping device is ineffective below a certain Reynolds number, depending on thickness and position of the device. Extensive tests, including flap deflections, showed that a zig-zag tape of 0.5 mm thickness, running form the

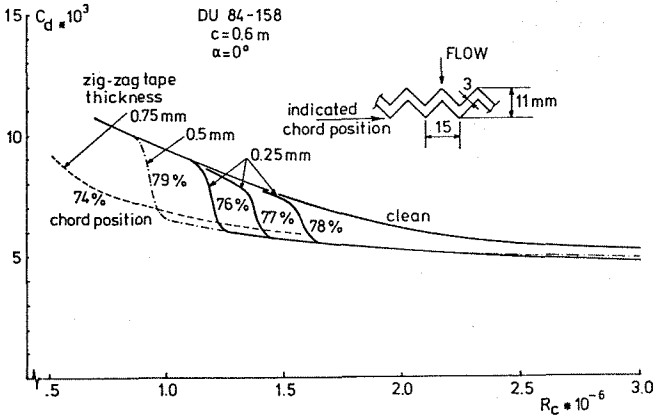

Fig. 4 Effect of position and thickness of zig-zag tape on drag

wing root (at 77%c) to the tip (at 74%c) may be expected to function very well at all practical flight conditions.

After the tests our attention was drawn to the work of Hama [5], where a row of thin triangular patches is proposed as being a "simple yet better way of tripping laminar boundary layers than any other known stimulation device". It is argued [6] that this device incorporates the favourable properties of both the two-dimensional element (which produces a larger perturbation in velocity than a three-dimensional element of the same size) and the three-dimensional element (which produces vortices that will go turbulent quicker than will two-dimensional disturbances). The minimum size of a trip required to result in transition at the trip without incurring undue extra drag to it, is characterized by a critical roughness Reynolds number R_k of about 300 for two-dimensional and 600 for three-dimensional roughness [7]. Analysis of

the measurements on DU 84-158 showed a mean critical roughness Reynolds number for zig-zag tape of 175, which confirms the effectiveness of this type of triangular tripping device.
The traces of the vortices produced by the zig-zag tape are clearly visible in fluorescent oil flow patterns, Fig. 5.

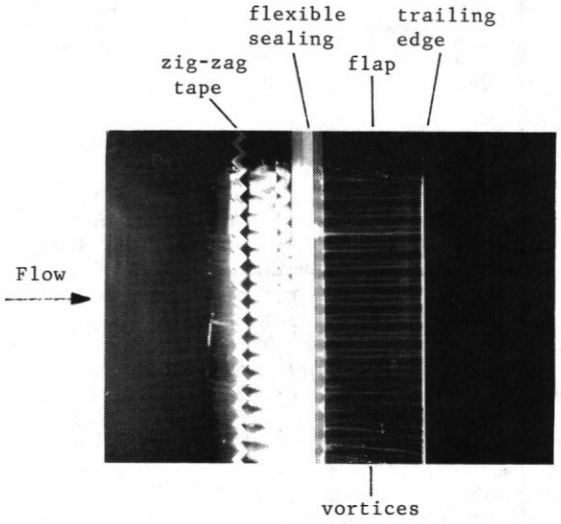

Fig. 5 Fluorescent oil flow pattern with zig-zag tape

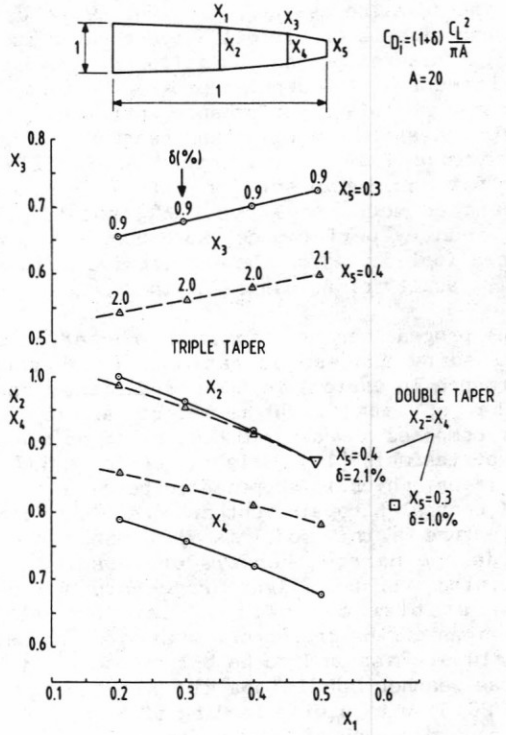

Fig. 6 Double and triple taper wings producing least induced drag

Planform

To find the planform for double- and triple taper wings which produce the least induced drag, Dr. J.L. de Jong of the Eindhoven University of Technology, Department of Mathematics, developed a computer program to solve this linearly constrained minimization problem. The calculations are based on lifting-line theory assuming linear section lift data, the spanwise distribution of circulation is expressed in terms of Fourier series.
Fig. 6 shows results for an aspect ratio of 20 and taper ratio at the tip of 0.3 and 0.4. Starting with an arbitrary planform (with prescribed tip taper ratio) the calculation for the double taper wing converge to a single combination of inner wing taper and spanwise position of taper ratio change, which produces the least induced drag. In case of a triple taper wing, however, the results showed that many planforms have an induced drag deviating less than 0.1% from the least possible value. At equal tip taper the difference in induced drag between these double and triple taper wings is negligible. For construction ease it was decided to stick to the double taper wing.
To take profile drag into account and to estimate roll control at stall conditions, the characteristics of several wings with aspect ratio 22.5 were calculated by the method of Sivells and Neely [8], using the measured airfoil data. Starting with the double taper wing with tip taper ratio 0.3 of Fig. 6, systematic variations with respect to taper ratio and washout in the inner and outer wing were studied. Taking additional twist due to aerodynamic load into account, the double taper wing previously mentioned with a washout of -0.85 degrees in the outer wing, showed the least total drag at all lift coefficients. In addition adequate roll control at stall conditions is expected due to the measured aileron effectiveness.

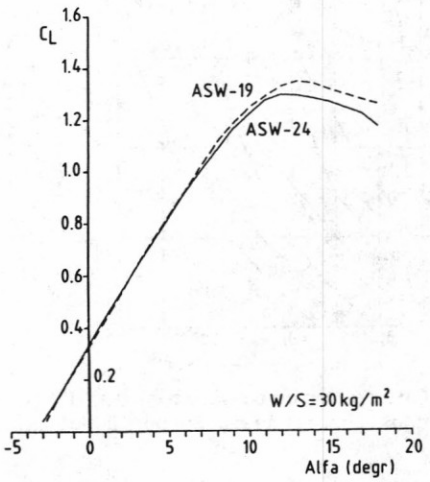

Fig. 7 Lift curves of the ASW-19B and ASW-24 wing

The lift curve of the ASW-24 wing is shown in Fig. 7; except for a slightly lower maximum lift coefficient the curve is similar to the ASW-19B wing lift curve (which has a very gentle stall).

Aspect ratio

As previously described, the new airfoil leads to improved performance at interthermal penetration speeds, where more than 40% of the sailplane drag is due to wing profile drag. The most effective way to reduce the wing drag coefficient at low speed climbing conditions, where more than 50% of the sailplane drag is due to induced drag,

is to increase the aspect ratio. Ref. 9 illustrates these effects of airfoil, aspect ratio as well as weight alterations on the sailplane speedpolar, calculated with a computer program developed for parametric sailplane performance optimization. In recent years this program has been extended with the previously mentioned method of Sivells and Neely for nonlinear section lift data, and with the weather model of Küpper [10] to calculate cross country performance. Moreover, the program has been implemented on the interactive CAD system of DUT, Faculty of Aerospace Engineering.

The program was used to study the effects of wing loading and aspect ratio on cross country performance in various weather conditions, assuming that optimum flight techniques are employed. Küpper composed a weather model, based on measurements of thermals [11], flight experience and some assumptions, which is supposed to be relevant for normal central European weather conditions. Essential feature of this model is that the strengths of wide and narrow thermals are assumed to be distributed over the flight trajectory according to the statistical normal distribution. The proportions of the trajectory with wide and narrow thermals are assumed to be 85% respectively 15%. In these weather conditions the ASW-19B (aspect ratio 20.5) with a wing loading of 32 kg/m^2 has a cross country speed of 70.2 km/hr.

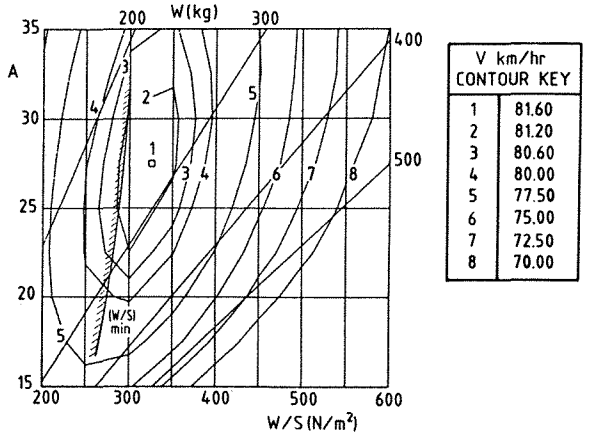

Fig. 8 Cross country speeds for ASW-24 configurations in Küpper's weather model

Fig. 8 shows the results for the ASW-24 configuration where the wing loading and aspect ratio are varied; the tailplanes are adjusted to the wing aspect ratio [9]. As shown, the optimal aspect ratio is 27.5 at a wing loading of 32.5 kg/m^2, and the cross country speed is 81.6 km/hr. With the wing loading and aspect ratio of the ASW-19B previously mentioned the cross country speed is only 2% lower, 80 km/hr, which indicates the flatness of the optimum.

Earlier studies, based on simpler weather models, resulted in an optimal aspect ratio between 15 and 20 [11-15]. Analysis showed that the wide thermals, which are present over a relatively large proportion of the trajectory in Küpper's model, ask for high aspect ratios. Moreover, the model is composed such that variation of the trajectory proportions with wide and narrow thermals has no effect on the cross-country speed

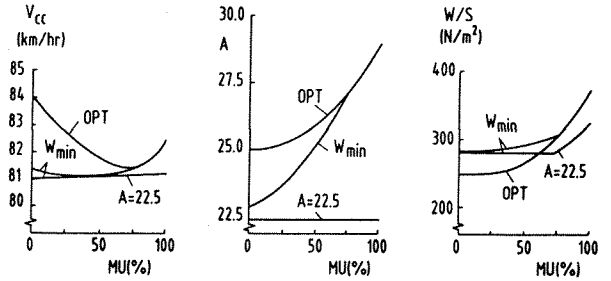

Fig. 9 Cross country speed, aspect ratio and wing loading at various weather models

of the typical Standard Class sailplane (A = 20, W/S = 32 kg/m^2) which was used to implement flight experience in the weather model. However, such alternatives of the weather model ask for other optimal combinations of aspect ratio and wing loading. As shown in Fig. 9, a decrease of the proportion with wide thermals, denoted by MU, (and increase of the proportion with narrow thermals, 1-MU) results in lower optimal aspect ratios and corresponding wing loadings. However, the wing loadings become unpracticably low; in these cases the (estimated) minimum possible wing loading, Fig. 8, determines the maximum attainable cross-country speed and corresponding aspect ratio. The flattness of the optimum, as previously noted, explains the good performance of a wing with aspect ratio 22.5 at corresponding optimal or minimal wing loading.
A further study with eight different weather models, composed by varying the strength of the narrow and wide thermals and their proportion of the trajectory such that the cross-country speed of the typical Standard Class sailplane remained constant again, resulted in optimal aspect ratios between 24 and 27.5 at wing loadings between 25 and 30 kg/m^2. Taking minimum practical wing loadings into account, the conclusion was the same as before.
Stronger weather conditions ask for lower aspect ratios and higher wing loadings. Again, the conclusion was that an aspect ratio of 22.5 combined with the proper wing loading (water ballast) give cross country speeds which differ negligibly from the optimal values.
All in all, an aspect ratio of 22.5 provides for an excellent compromise in various weather conditions.

Fuselage

In a previous research project eight sailplane wing-fuselage combinations were windtunnel tested at LSL [16]. The combinations were obtained by combining three different fuselages with the central section of a wing at various positions, Fig. 10. The basic fuselage, no. 1, was a 1:3 scale model of the ASW-19B fuselage. Fuselage 2 and 3 had the same forebody as fuselage 1 but differed in contraction ratio and had a 1/3 thinner tailboom. The wing segment had the Wortmann airfoil FX62-K-131/17.

Comparison of the drag results showed a significant and essentially equal drag reduction for the waisted fuselages 2 and 3 with respect to fuselage 1, primarily due to the reduction in wetted surface. Considering friction and pressure

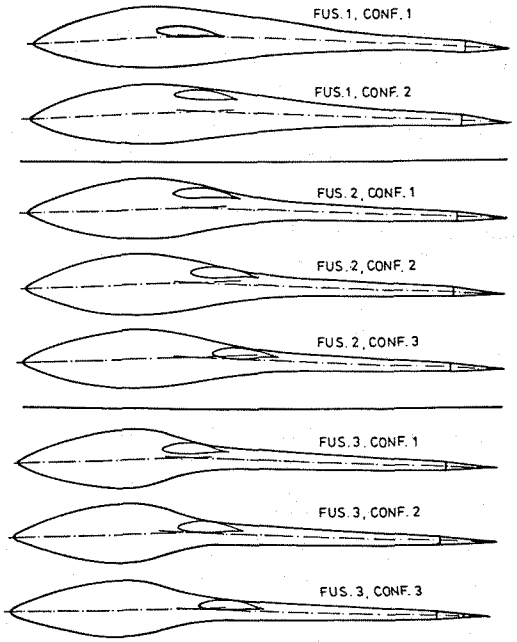

Fig. 10 Wing-fuselage combinations tested at LSL

drag the optimum contraction ratio is obviously closely met. Therefore, these contractions served as a guideline to the design of the ASW-24 fuselage contraction.
The windtunnel results also showed the importance of streamline shaping, i.e. fitting the forebody to the streamlines of the wing to minimize crossflow effects. This crossflow effectively increases the angle of attack at the wing root area, thus causing drag increase and eventually early separation at higher angles of attack. Also, at a rearward position of the wing the accumulation of boundary layer material coming from the forebody and flowing over the upper surface of the fuselage, running up against the successive adverse pressure gradients of the fuselage contraction and induced by the wing, leads to thick boundary layers and consequently higher drag. Therefore, the very small drag reduction measured for a rearward wing location at low lift coefficients does not outweigh the drag increase at higher lift coefficients (not to mention the structural consequences of negative wing sweep for centre of gravity reasons).

The forebody centerline of the ASW-24 fuselage is parallel to the streamlines of the wing at a lift coefficient of 0.85. The upper and lower forebody contours are obtained by transforming the Wortmann FX71-L-150/30 low drag airfoil into a threedimensional body with approximately the same super-velocity at maximum thickness [17] and laying off the resulting smooth thickness distribution perpendicular to the body centerline. A similar procedure is followed for the width at the forebody centerline. The cross sections of the fuselage are defined by a mathematical expression with continuous curvature (for smooth velocity distributions) along the contour.
The fuselage centerline behind the wing is parallel to the streamlines of the wing at a lift coefficient of 0.6, and the dimensions of the tailcone are limited by structural stiffness requirements.

Overall, the wetted surface of the fuselage is about 20% less than other modern production type Standard Class sailplanes.

Wing-fuselage combination

In order to check the pressure distributions on the wing and fuselage and to study wing-fuselage interference effects, a first-order panel method developed at NLR [18] has been applied. Considering that viscous effects are not taken into account, the qualitative agreement between measured and calculated pressure distributions for attached flow conditions is shown to be excellent [18, 19].

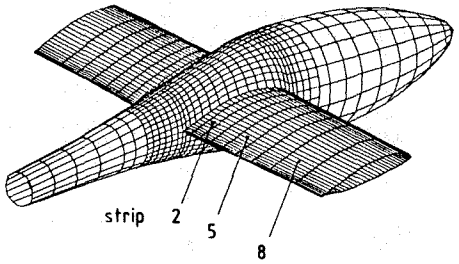

Fig. 11 Part of panel scheme of ASW-24 wing-fuselage combination

Fig. 11 shows the interesting part of the paneled wing-fuselage combination, produced by means of the CAD system. The density of the panels in the junction area was increased to obtain detailed pressure distributions.

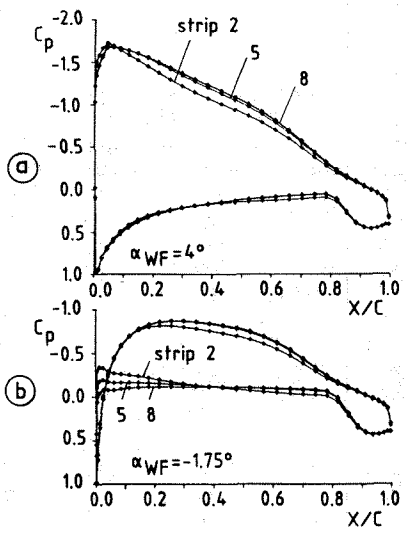

Fig. 12 Pressure distributions of wing strips in the wing root area

Fig. 12a and 12b show pressure distributions of wing strips located within one fuselage diameter from the junction. The consequence of fitting the fuselage forebody to the streamlines of the wing at a higher lift coefficient - thus avoiding additional suction peaks at the leading edge, Fig. 12a - is an increased crossflow effect at a low lift coefficient, indicated by the lower surface pressure distributions in Fig. 12b. Hence,

at high speed conditions when the wing airfoils approach the lower end of the low drag bucket a small part of the wing next to fuselage operates below the low drag bucket. This effect was also noticed in the drag measurements for all the combinations mentioned before.

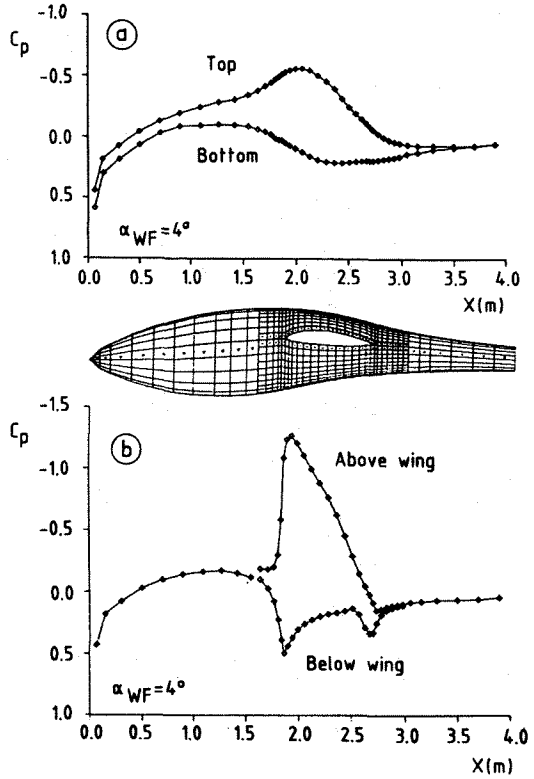

Fig. 13 Pressure distributions along top, bottom and side of the fuselage

Fig. 13a shows pressure distributions along the top and bottom of the fuselage at a lift coefficient of about 1.1. The pressure gradients due to fuselage contraction and induced by the wing on the top of the fuselage are properly combined to postpone transition. The flat pressure distribution on the bottom of the fuselage, below the pilot's seat, may cause earlier transition. To assure an aft position of transition the bottom line and cross sections were slightly modified (not shown here). Fig. 13b shows the pressure distribution on the side of the fuselage and along a row of panels running just above and below the wing. Despite the pressure rise induced by the wing upper surface, oil flow studies on the eight combinations indicated no separation problems on the fuselages. On the contrary, the pressure rise induced by the wing root stagnation pressure causes the laminar forebody flow to become turbulent first and then to separate; a separation line around the junction is observed in the oil-flow patterns, its position depends on the angle of attack. The separated flow rolls up into a system of vortices wrapped around the wing root. The experiments also indicated that separation can be expected due to the steep pressure rise induced by the airfoil rear lower surface.

To improve the flow conditions at the junction, the wing has been modified in the wing root area. A small fairing with 7% chord extension has been applied where the wing is lofted towards a wing root airfoil designed to be suitable for turbulent flow conditions (at least in the two-dimensional case). In comparison to the wing airfoil, turbulent separation on the root airfoil upper surface is predicted to start at a higher lift coefficient, and a steep pressure rise on the rear lower surface has been avoided. Flight tests will have to show if this fairing is adequate. Meanwhile, research on the design of proper wing-fuselage junctions continues at LSL; the imperfections traced by the experimental and theoretical methods are - more or less - present on all existing sailplanes.

Tailplanes

The horizontal and vertical tailplane operate at conditions where special measures have to be taken to avoid detrimental laminar separation bubbles. Wortmann applied extensive instability regions on his well-known airfoils FX71-L-150/20, /25 and /30, designed for tailplane application [20]. The success of artificial tripping devices to avoid these bubbles, thus making longer laminar flow regions possible on sailplane wings, is the obvious reason to apply this technique also in designing new airfoils for the ASW-24 tailplanes [21].

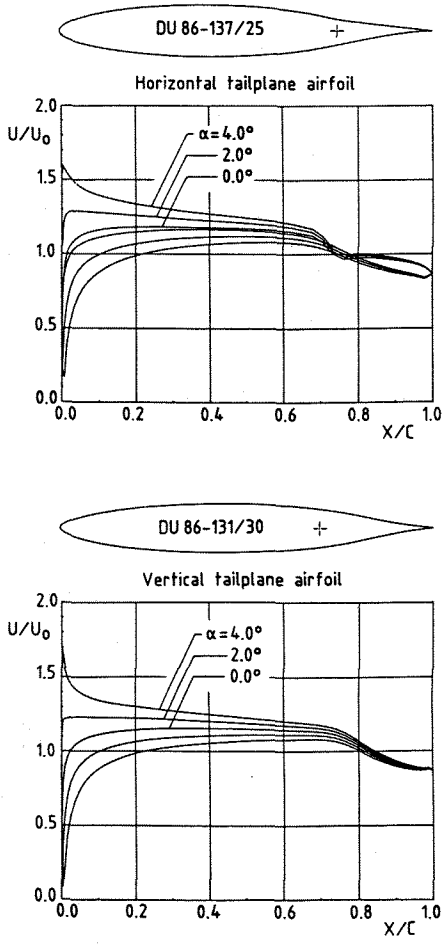

Fig. 14 Tailplane airfoils and potential flow velocity distributions

The desired width of the low drag bucket for the horizontal tailplane airfoil was derived by calculating the operating range of angles of attack and elevator deflections in straight and circling flight at forward and rearward c.g.-positions [22]. For safety reasons, for instance to counteract undesired motions of the airplane due to instationary cable towing, $c_{\ell_{max}}$ values were required to be comparable to the values of the Wortmann tailplane airfoils. The desired width of the low drag bucket for the vertical tailplane airfoil was derived from slip and rudder deflection measurements with an ASW-20 in thermal flight conditions.
All modern sailplanes have a T-tail configuration where the leading edge of the horizontal tailplane midspan section projects in front of the vertical tailplane. Similar to the wing-fuselage junction flow, the laminar boundary layer on the lower surface of the horizontal tailplane turns turbulent and separates as it approaches the vertical tailplane stagnation, and the separated flow rolls up in a system of vortices wrapped around the junction. Separated flow is observed at the rear part of the corner [23].

To improve the flow conditions at the junction the leading edges of the ASW-24 horizontal and vertical tailplane coincide and steep airfoil pressure gradients are avoided. The upper surface of the horizontal tailplane airfoil, however, was designed to avoid steep pressure gradients on the elevator at downward deflections (for $c_{\ell_{max}}$ reasons), hence, the horizontal tailplane airfoil is not symmetrical. Fig. 14 shows the horizontal tailplane airfoil (thickness 13.7%c, elevator depth 25%c) and the vertical tailplane airfoil (thickness 13.1%c, rudder depth 30%c) as well as some potential flow velocity distributions indicating that laminar flow is intended up to 65% respectively 70% of the chord.
Windtunnel tests on a part of the horizontal tailplane are currently being evaluated. The results show that the functions of zig-zag tape and flexible sealings can be integrated by cutting zig-zags in the leading edge of the sealings stuck on the surface. With zig-zags at 62%c (thickness 0.5 mm) the drag is about 10% lower and $C_{\ell_{max}}$ only 5% lower than FX71-L-150/25.

3. Structural design

Materials

Due to the desired high aspect ratio and low wing loading (without water ballast) the ASW-24 has to be lighter in weight than its forerunner ASW-19B. This weight reduction is possible as new materials are available and approved for sailplane design. In the past the prices of carbon and aramide fibers were decreasing while the price of glass fiber went up slowly. It is expected that this trend will continue so that the advantages of the new materials will be available at a fair price in the future.
Fig. 15 shows the data for the pure fibers as provided by the manufacturers [24-26] and Fig. 16 shows the fiber properties verified in laminates by the fabric industry [27]. The data show that carbon fiber is most favourable for light-weight

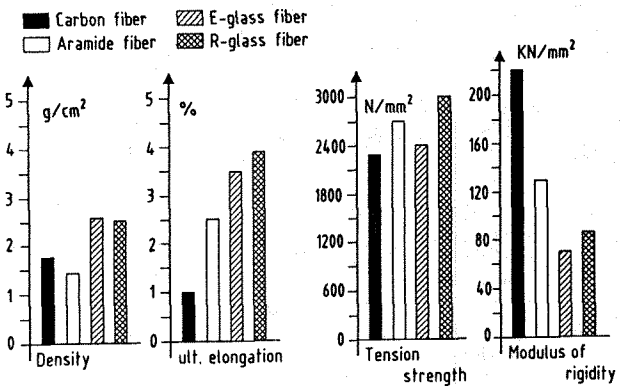

Fig. 15 Properties of pure fibers

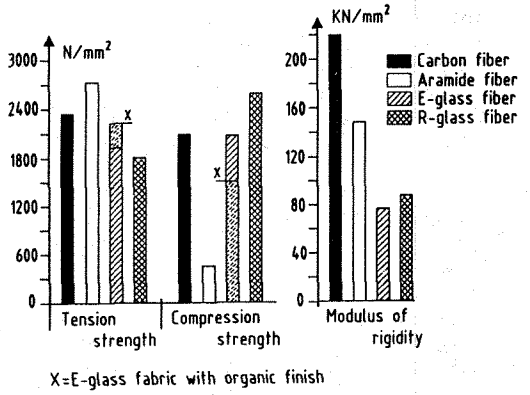

Fig. 16 Fiber properties verified in laminates

and stiff structures whereas aramide is handicapped because of its low compression strength.
All German sailplane manufacturers as well as University Institutes, Akafliegs, material suppliers and the airworthiness authority are members of a study group (ANF) which is chaired by DFVLR. The material properties given in Table 1 and 2 for unidirectional and bidirectional fiber epoxy laminates have been evaluated by this study group [28]; the values cover fatigue due to 6000 or 12000 flying hours and apply to certain fiber/resin combinations as well as special manufacturing and postcure procedures. The data may appear very conservative; the group will continue the tests to get higher values and more flying hours.

Wing

As shown in Table 1, the most favourable material for spar flanges is carbon fiber. The specific strength, which includes the different densities of the laminated material, is for carbon/epoxy nearly twice as good as for glass, whereas aramide is still handicapped because of its poor compression strength.
It is important that the skins of the wing are optimized as they represent a large amount of the structural weight of this component. It should be realized that there are usually no strength problems with the skins whereas a certain torsional stiffness is required for performance reasons as well as to avoid adverse bending loads due to

	Carbon	Glass	Aramide
Fiber volume contents [%]	55,6	39,4	40
Density [g/cm^3]	1,52	1,73	1,28
Tolerable tension/ compression strength [N/mm^2]	633	375	100
Specific tolerable strength [km]	42,5	22,1	8,0

Table 1 Material properties of unidirectional fiber reinforced epoxy laminates

	Carbon	Glass	Aramide
Fiber volume contents [%]	35	35	35
Density [g/cm^3]	1,40	1,67	1,72
Specific fabric stiffness [km]	2050	830	1360
Weight factor for given stiffness	$42*10^{-5}$	$82*10^{-5}$	$67*10^{-5}$

Table 2 Material properties of bidirectional 45°/45° fiber fabric epoxy laminates

twist. Table 2 shows the decisive data for the skin materials. The specific fabric stiffness must be read as shear rigidity (Modulus X wall thickness in terms of conventional material, kp/cm) for a 45°/45° bidirectional fabric of 100 p/m^2 weight per area. The weight data are calculated for a rather low fiber volume contents of 35%, which can be easily achieved in thin, hand-lay-up laminates. For a given stiffness the carbon laminate has the lowest weight. However, the ASW-24 has such a lowly loaded wing skin that even the thinnest carbon material (which is not too expensive) is too thick. Moreover, this rather rough fabric would result in a bad surface. Hence, the second choice, which is the aramide skin, was selected for the ASW-24. Compared to a glass fiber skin the weight reduction is about 20%. Despite this weight saving the skin is 5% thicker, which is a noticeable gain for a better airfoil contour.
One of the reasons to use glass fibers for the shear webs of the spar, the root ribs and the stringers, is their cheapness. Looking closer into the problem of fatigue, it turns out that critical elongations must not be exceeded to avoid damage. Of course, this criterium only works within a certain range of fiber volume contents. Also the elastic properties of the design have to be adequate. For highly stressed components three elongations have to be considered, Fig. 17. In case of a typical carbon flange combined with a glass shear web 20% of the total tolerable elongation is due to elongation of the flange, 4% due to compression because of bending deformation and 76% due to shear. This is very favourable. On the other hand, in case of a carbon shear web more than 55% of the tolerable elongation would be used for unavoidable geometrical elongations so that much more carbon must be used to take the remaining shear load.

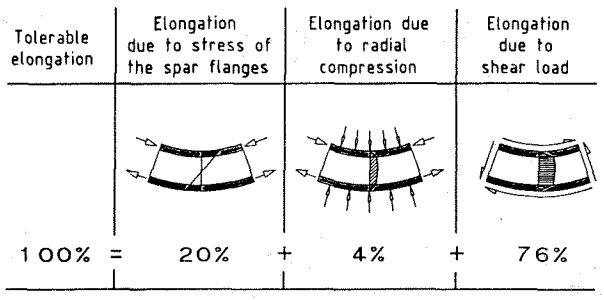

Fig. 17 Elongations of a typical spar with carbon flanges and glass shear web

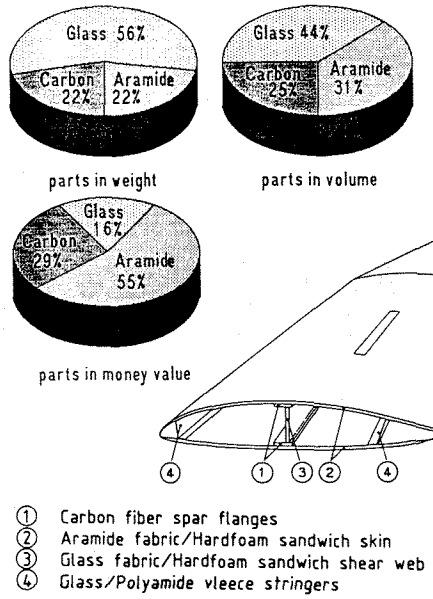

Fig. 18 Structural design and fiber contents of the wing

Fig. 18 shows the structural design of the wing and the fibers used for its construction, as previously described. In comparison to the glass fiber ASW-19B wing (125 kg without airbrake, aileron and waterbag), the ASW-24 wing (94.5 kg without airbrake, aileron and waterbag) is about 25% lighter. The ASW-24 wing however is designed to carry a 17% higher fuselage load due to the engine of the ASW-24E motorglider.

Fuselage

The fuselage structure of the ASW-24 cannot be directly compared in weight with the ASW-19B. It is really by some percent lighter but many comfort and safety features which have been incorporated, are heavy components, like airtight sealed landing gear box, suspension, hydraulic disc brake, oxygen-bottle box, second baggage compartment, battery box, etc.
For pilot's safety two new design features are incorporated to increase the crashworthiness. Fig. 19 shows the impact energy absorption of glass, aramide and carbon laminates; the glass fabric is still the best material. Fig. 20 shows the energy absorption of carbon/aramide hybrid

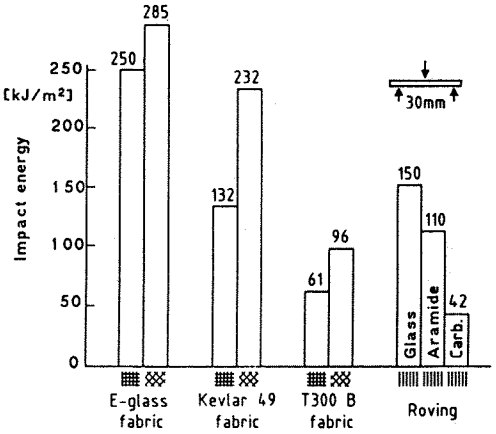

Fig. 19 Impact energy of epoxy laminates

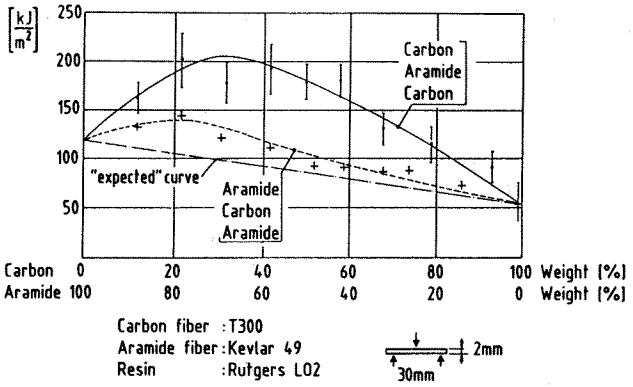

Fig. 20 Impact energy of hybrid laminates

laminates; the mixture of carbon and aramide is always better than expected. The best results are achieved when 70% of aramide fibers are sandwiched with 15% of carbon fibers on each outside. The major part of the ASW-24 rear fuselage is built like this. It is assumed that the same positive effect is achieved if glass replaces the aramide. Therefore glass/carbon hybrid laminates are used in the cockpit area as fiberglass has the highest energy absorption of all materials discussed here.
A second safety feature is the cockpit design itself; Fig. 21 shows the cross section of the ASW-24 fuselage and a conventional fuselage. Both designs give the same pilot's view to the side. However the new ASW-24 design has a 60% higher moment of inertia against bending loads at the cost of a slight weight increase when the same material thickness is used. In addition, the wall inside the cockpit is nearly straight which gives a much higher buckling stability than the more curved cockpit walls of conventional design.

Tailplanes

The horizontal tailplane structural design is similar to the wing except for the spar flange which is an unidirectional carbon fiber lay-up. The vertical tailplane will be redesigned as the first ASW-24 came out a bit noseheavy. In order to save production time the sandwich will be replaced by a heavier glassfiber shell.

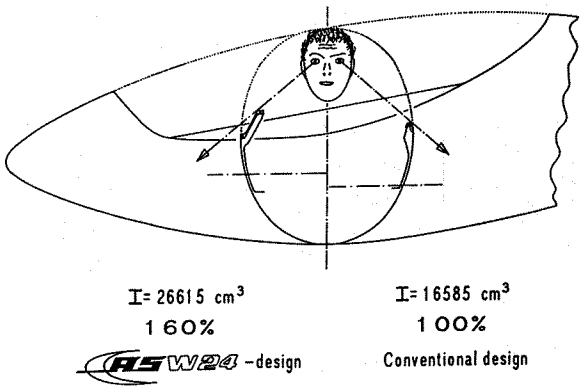

Fig. 21 Safety cockpit design

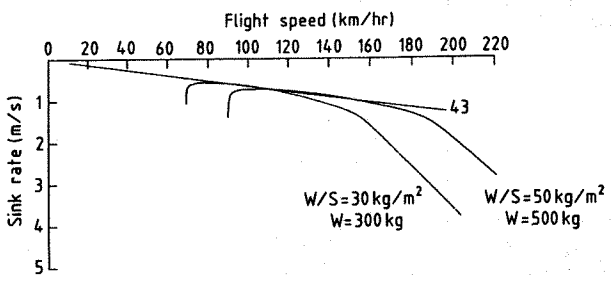

Fig. 22 Calculated performance of the Standard Class Sailplane ASW-24

4. Preliminary flight experience

First flight of the ASW-24 was on December 14th 1987, and the calculated performance of Fig. 22 have not been verified yet. However, comparison flights with modern sailplanes indicate that the performance of the ASW-24 in thermals is about equivalent, and at best glide and higher flight speeds the ASW-24 seems to perform closer to latest design FAI 15m Racing Class sailplanes with camber changing flaps (like ASW-20B and C) than to Standard Class sailplanes.
Obviously due to the clean aerodynamic design, the stall warning is little and in case of the ASW-24E motorglider probably hardly noticeable when the engine is operating. However, stall behaviour is extremely forgiving and stall control far better than required by JAR 22.
Nearly every pilot who noticed the unusually narrow chord of the ailerons was impressed by the effectiveness of the roll control, which holds in case raindrops or light icing deteriorate the laminar flow of the wing airfoil.

Acknowledgments

The authors are indebted to the colleagues at the Low Speed Laboratory for their support and assistance, to B. Oolbekkink, R.H.J. Oerlemans, L.R.J. Mulkens, J. Middel and S.J. Vermeer for their valuable contributions performed in the framework of their thesis work and to D. Somers of NASA Langley for drawing our attention to the work of Hama.

References

1. Boermans, L.M.M., Selen, H.J.W.: Design and tests of airfoils for sailplanes with an application to the ASW-19B. ICAS-paper 82-5.5.2, 1982.
2. Horstmann, K.H., Quast, A., Boermans, L.M.M.: Pneumatic turbulators - A device for drag reduction at Reynolds numbers below 5.10E6 AGARD CP-365, paper 20, 1984.
3. Ingen, J.L. van, Boermans, L.M.M.: Aerodynamics at low Reynolds numbers: A review of theoretical and experimental research at Delft University of Technology. Proceedings of the International Conference on Aerodynamics at Low Reynolds Number, Royal Aeronautical Society, London, October 1986.
4. Althaus, D.: Stuttgarter Profilkatalog I. Institut für Aero- und Gasdynamik der Universität Stuttgart, 1972.
5. Hama, F.R.: An efficient tripping device. Journal of the Aeronautical Sciences, Vol. 24, no. 3, 1957.
6. Smith, A.M.O., Clutter, D.W.: The smallest height of roughness capable of affecting boundary layer transition. Journal of Aerospace Sciences, april 1959.
7. Young, A.D., Paterson, J.H.: Aircraft Excrescence Drag. AGARDograph 264, 1981.
8. Sivells, J.C., Neely, R.H.: Method of calculating wing characteristics by lifting-line theory using nonlinear section lift data. NACA TN No. 1269, 1947.
9. Boermans, L.M.M.: Development of a computer program for parametric sailplane performance optimization. OSTIV Publication XV, 1980.
10. Küpper, T.: Reisegeschwindigkeit von Segelflugzeugen unter Berücksichtigung von statistischen Aufwindstärken. DFVLR-FZ Braunschweig, Unpublished students-thesis, 1984.
11. Horstmann, K.H.: Neue Modellaufwindverteilungen und ihr Einfluss auf die Auslegung von Segelflugzeugen. OSTIV Publication XIV, 1976.
12. Irving, F.G.: Computer analysis of the performance of 15 m sailplanes using thermals with parabolic velocity distributions. OSTIV Publication XI, 1970.
13. Irving, F.G.: Computer analysis of the performance of 15 m sailplanes.NASA CR-2315, 1972.
14. Eppler, R.: When should we use water ballast? NASA CR-2315, 1972.
15. Boermans, L.M.M.: Soaring flight optimization theory and an application in sailplane design. NVvL-Annual Report 1978.
16. Boermans, L.M.M., Terleth, D.C.: Windtunnel tests of eight sailplane wing-fuselage combinations. OSTIV Publication XVII, 1983.
17. Galvao, F.L.: A note on low drag bodies. OSTIV Publication X, 1968.
18. Labrujere, Th.E., Loeve, W., Slooff, J.W.: An Approximate Method for the Calculation of the Pressure Distribution on Wing-Body Combinations at Subcritical Speeds. AGARD CP 71-11, 1970.
19. Baston, A., Lucchesini, M., Manfriani, L., Polito, L., Lombardi, G.: Evaluation of pressure distributions on an aircraft by two different panel methods and comparison with experimental measurements. ICAS-86-1.5.3, 1986.
20. Wortmann, F.X.: Symmetrical airfoils optimized for small flap deflections. OSTIV Publication XII, 1972.
21. Boermans, L.M.M.: Airfoil design for the horizontal tailplane of a sailplane. Delft University of Technology, Low Speed Laboratory. Internal Report LSW 86-2, 1986.
22. Stich, G.: Das gedämpfte Höhenleitwerk in Kreisflug. OSTIV Publication XVI, 1981.
23. Lautanala, L.: Flow visualization in the horizontal and vertical stabilizer joint area in a glider aircraft. Bericht Idaflieg Wintertagung, Heft VIII, 1982.
24. Enka AG: Data of Twaron (Aramide) fibers and TOHO-carbon fibers (according to quality control certificates).
25. Du Pont: Kevlar 49 data manual.
26. Sigri GmbH: Data of NF carbon fibers (quality control certificates).
27. Interglas GmbH: Data of various woven filament fiber materials.
28. ANF-Study group/LBA: RHV-Richtlinien.
29. Waibel, G.: Substantiation of airworthiness for the ASW-20, ASW-22 and ASW-24 gliders.